CEAS Space J (2016) 8:65–75
DOI 10.1007/s12567-015-0108-y

ORIGINAL PAPER

Experimental investigation on IXV TPS interface effects in Plasmatron

Giuseppe Ceglia[1] · Eduardo Trifoni[1] · Jean-Baptiste Gouriet[2] · Olivier Chazot[2] · Vincenzo Mareschi[3] · Giuseppe Rufolo[4] · Giorgio Tumino[5]

Received: 15 May 2015 / Revised: 16 August 2015 / Accepted: 11 November 2015 / Published online: 20 November 2015

Abstract An experimental investigation related to the thermal protection system (TPS) interfaces of the intermediate experimental vehicle has been carried out in the Plasmatron facility at the von Karman Institute for fluid dynamics. The objective of this test campaign is to qualify the thermal behaviours of two different TPS interfaces under flight representative conditions in terms of heat flux and integral heat load (~180 kW/m^2 for 700 s). Three test samples are tested in off-stagnation configuration installed on an available flat plate holder under the same test conditions. The first junction is composed of an upstream ceramic matrix composite (CMC) plate and an ablative P50 cork composite block separated by a gap of 2 mm. The second one is made of an upstream P50 block and a downstream ablative SV2A silicon elastomer block with silicon-based filler in between. A sample composed of P50 material is tested in order to obtain reference results without TPS interface effect. The overheating at the CMC–P50 interface due to the jump of the catalytic properties of the materials, and the recession/swelling behaviour of the P50–SV2A interface are under investigation. All the test samples withstand relatively well the imposed heat flux for the test duration. As expected, both the ablative materials undergo a thermal degradation. The P50 exhibits the formation of a porous char layer and its recession; on the other hand, the SV2A swells and forms a fragile char layer.

Keywords Ground testing · Thermal protection system · Gas-surface interaction · Catalysis

This paper is based on a presentation at the 8th European Symposium on Aerothermodynamics for Space Vehicles, March 2–6, 2015, Lisbon, Portugal.

✉ Giuseppe Ceglia
g.ceglia@cira.it

Eduardo Trifoni
e.trifoni@cira.it

Jean-Baptiste Gouriet
gouriet@vki.ac.be

Olivier Chazot
olivier.chazot@vki.ac.be

Vincenzo Mareschi
vincenzo.mareschi@thalesaleniaspace.com

Giuseppe Rufolo
g.rufolo@cira.it

Giorgio Tumino
giorgio.tumino@esa.int

[1] Centro Italiano Ricerche Aerospaziali, via Maiorise, 81043 Capua, Italy

[2] Von Karman Institute, Chausée de Waterloo 72, 1640 Rhode-St-Genèse, Belgium

[3] Thales Alenia Space Italia, Strada Antica di Collegno 253, 10146 Turin, Italy

[4] CIRA/ASI Technical Assistance to ESA, Paris, France

[5] European Space Agency, 8-10 rue Mario Nikis, 75738 Paris, France

1 Introduction

On 11 February 2015, the European Space Agency (ESA) intermediate experimental vehicle (IXV), led by Thales Alenia Space-Italy (TAS-I) as prime contractor, successfully completed its 100 min space mission. In particular, European capabilities in hypersonic unpowered manoeuvring re-entry flight of a lifting configuration have been verified. This vehicle is an atmospheric re-entry demonstrator conceived to perform a sub-orbital flight and to re-enter the atmosphere at 7.5 km/s speed. During its mission, the vehicle served as an in-flight laboratory for the qualification

of vehicle subsystems and systems, and to provide another source of data on fundamental hypersonic phenomena for validation of tools, databases and design processes.

Space vehicles re-entering in a planetary atmosphere undergo severe environment flight conditions due to aero-thermodynamic loads impinging on the exposed surfaces [1]. Thus, development of specific thermal protection system (TPS) is required.

Depending on the flight altitude and Mach number, the flow around the vehicle is characterized by the presence of dissociation and ionization phenomena due to the conversion of kinetic energy into thermal energy [2]. The environment across the shock waves results in a chemically reactive flow interacting with the walls. When dissociated species approach the heat shield, this interaction influences their recombination in exothermic reactions depending on the catalytic nature of the TPS. In this scenario, catalytic processes drive the concept and design of the TPS materials. Indeed, the TPS material influences the performance of the heat shield promoting the catalytic processes along with other mechanisms, i.e. radiative effects and oxidation/nitridation phenomena [3].

The combination of different TPS materials in complex assemblies introduces variations of heat flux distribution due to discontinuities of catalytic properties at the interfaces [4]. Nearby to these interfaces, overheating effects can be induced by variations of recombination rate of the reacting species.

The scope of this work is related to the activities of the TPS qualification for the IXV project. The objective of this test campaign is to collect plasma wind tunnel data to investigate two different material interfaces used in IXV TPS. In particular, the first junction is composed of ceramic matrix composite (CMC) material, located upstream to an ablative material P50 cork composite. The second junction is based on two ablative materials P50 and SV2A silicon elastomer. The sample assembling, the operating conditions and the test procedure are described in the following sections. Furthermore, the test results are investigated in terms of TPS performance qualification.

2 Experimental setup

The experiments are conducted in the Plasmatron facility [5] at the von Karman Institute for Fluid Dynamics (VKI). The Plasmatron is a high enthalpy wind tunnel, equipped with a high power, high frequency and high voltage (1.2 MW, 400 kHz, 2 kV) solid state generator.

A 160 mm diameter plasma torch provides a plasma jet in a 2.5 m long, 1.4 m diameter test chamber. A holding probe allows for the investigation of TPS materials and a stagnation point (SP) heat flux probe is used for the flow characterization. They are mounted on two water-cooled arms that can be injected into and out of the flow by a hydraulic displacement mechanism.

The experimental campaign is carried out by applying off-stagnation testing methodology described in [6].

Off-stagnation configuration is realized by using a flat plate (FP) probe. Such a probe offers flight representative test conditions for boundary layer investigation. The FP consists of a copper plate mounted on a swinging-in water cooled arm. The plate has a 12.5 mm radius rounded nose. The plate spanwise dimension is ~200 mm. A groove with a width of 30 mm, a length of 189 mm and a depth of 22.5 mm allows for the installation of a test sample or a linear calorimetric element [7].

Viladegut [7] performed calibration tests by using intrusive measurements techniques to characterize the flow field at different operating conditions. Several off-stagnation heat flux distributions have been measured at the chamber with a static pressure of $P = 1500$ Pa for different mass flow rates and stagnation heat flux. One of these distributions, i.e. air mass flow of 16 g/s and stagnation heat flux Q_{st} of 597 kW/m^2, matches with the present test requirements. The test operating requirements reproduce flight representative conditions in terms of heat flux and integral heat load, i.e. ~180 kW/m^2 fully catalytic cold wall condition at the TPS interface for 700 s. The test conditions are summarized in Table 1. The corresponding

Table 1 Operating conditions

Static pressure	1500 Pa
Gas mixture	Standard air
Mass flow rate	16 g/s
Stagnation heat flux	597 kW/m^2
Dynamic pressure (measured in [7])	336 Pa
Total enthalpy	11.7 MJ/kg
Velocity	840 m/s
Temperature	4715 K
Off-stagnation heat flux at $x = 110$ mm	180 kW/m^2

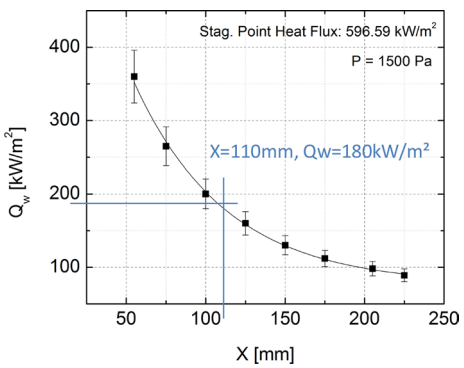

Fig. 1 Off-stagnation heat flux distribution with respect to the axial coordinate ($Q_{st} = 597$ kW/m^2, $P = 1500$ Pa) [7]

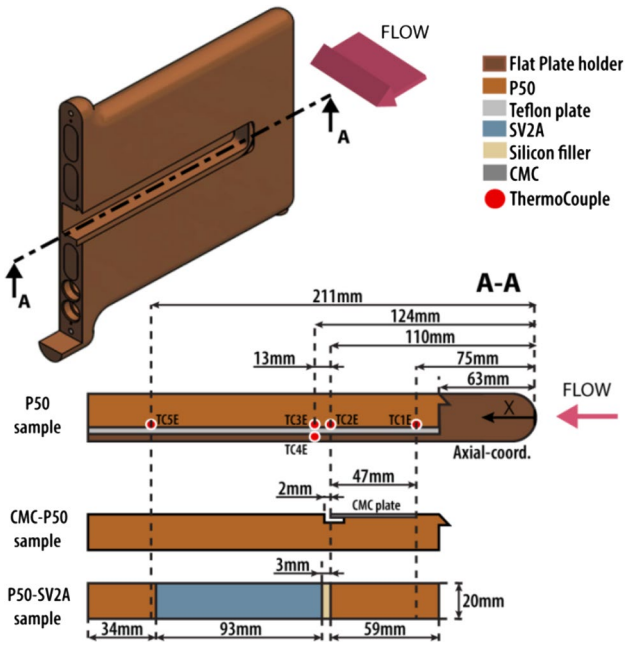

Fig. 2 Schematic of the holder and samples: *red circles* indicate the position of the contact thermocouples (cut view along the *centreline*)

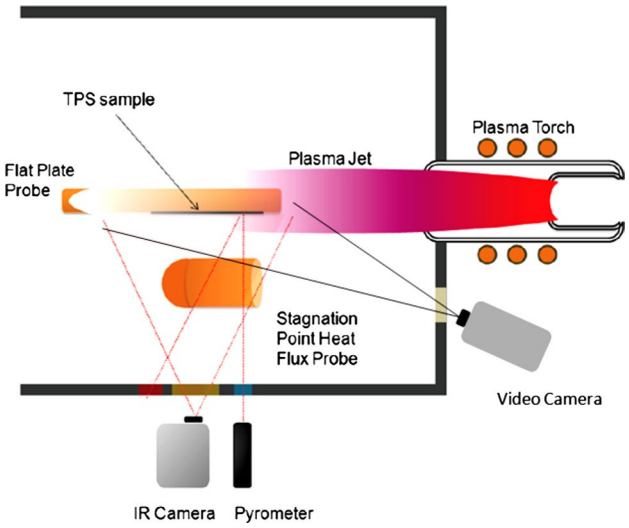

Fig. 3 Schematic view of the experimental setup

streamwise distribution of the heat flux is plotted in Fig. 1, extracted from [7].

In Fig. 2, four type-E thermocouples (TCs), TC1E, 2E, 3E and 5E, measure the contact temperature on the back wall of the test sample at different positions. An additional one, i.e. TC4E, is positioned on the other side of a Teflon plate in order to monitor the temperature of the water-cooled flat plate during the experiments. The error for a standard grade E-type thermocouple is ±1.7 °C or ±0.5 % of the measurement temperature; the effect of other parameters (contact, heat conduction etc.) on the overall uncertainty of the thermocouples measurement has not been evaluated. The positions of the TCs along the centreline of test samples are shown in Fig. 2. The TCs are installed on the Teflon plate into a groove built along the centreline.

A schematic view of the experimental setup is depicted in Fig. 3 with the respective positions of the optical instruments and water cooled probes, i.e. FP and the SP probes. Three optical accesses at Plasmatron test chamber enable non-intrusive diagnostics to probe the flow and the test samples: the lateral windows allow for perpendicular side views of the plasma jet and probes, and the torch-side window allows for a frontal oblique view of the TPS surface.

A two-colour pyrometer, an infrared (IR) camera and a video camera have been mounted in correspondence of these optical accesses. The two-colour pyrometer points to the surface sample at location ~124 mm from the leading edge of the flat plate, i.e. in correspondence of the same streamwise position of the thermocouples TC3E and TC4E. The model is the Marathon Series MR1SB (Raytek Corp., Santa Cruz, CA) with an operating temperature range between 700 and 1800 °C. Its detector is a Si/Si layer detector with a spectral nominal response at 1.0 µm. The spectral band response for the two-colour mode is 0.75–1.1 µm for the large band and 0.95–1.1 µm for the narrow band; Panerai [3] has estimated its overall uncertainty at ±10 % in the lowest temperature range. A quartz window of 18 mm thick is located at ~1.0 m from the test sample. The size of the target spot at 1.0 m from the target is ~12 mm (magnification of 82:1). The pyrometer is inclined of ~9° with respect to the surface normal. A blackbody reference source (Landcal R1500T, Land Instruments International) has been used to calibrate the two-colour pyrometer taking into account the presence of the window through the optical path. The temperature measured by the two-colour pyrometer is considered as real surface temperature being emissivity independent. In order to measure the distribution of the temperature over the surface sample, the test models are observed by the IR camera (ThermaCAM SC3000, FLIR systems) with a 320 × 240 resolution and a maximum spectral sensitivity at 8–9 µm. The IR camera measures in the range of temperature between 350 and 1500 °C with an acquisition rate of 50 Hz. The IR thermogram is imaged through a KRS-5 window of 18 mm thickness located at ~1.0 m from the test sample. The sensor is inclined at ~3.5° with respect to the surface normal. The same calibration procedure performed for the two-colour pyrometer has been applied for the IR camera. The emissivity ε_{IR} set in the IR camera, which is indeed a spectral directional emissivity, has been kept constant and is equal to 0.8 for all the tests.

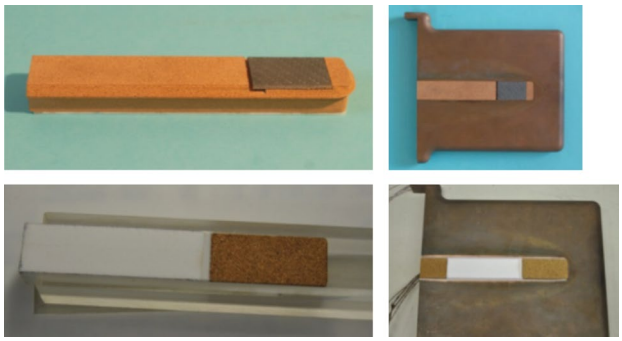

Fig. 4 CMC–P50 (*top*) and P50–SV2A (*bottom*) samples before (*left*) and after installation (*right*)

2.1 Test samples

Three different test samples are investigated under the same test conditions. The first test sample is composed of P50 cork composite material produced by Amorin Cork Composite [8]. The second sample is composed of a base made in P50 cork and a plate of 47 mm streamwise length made of Sepcarb-Inox® L6 C/SiC composite material manufactured by Safran Herakles. As for the P50 sample, a dovetail joint is the technical solution for the fixation of the P50 base and of CMC plate on the FP holder. A gap of 2 mm is provided between CMC and P50 materials. This junction is at 110 mm from the leading edge of the FP holder. It is worth mentioning the internal geometry of the gap reproduces the TPS flight interface configuration (Fig. 2). Figure 4 (top) shows the CMC–P50 sample before (left) and after installation on FP holder (right).

The third sample is composed of two different ablative materials, i.e. P50 and a silicone elastomer-based material SV2A manufactured by AVIO. They compose two parallelepiped blocks installed in series as shown in Fig. 2. P50 block is located upstream with respect to the SV2A block. The width and depth of these elements are, respectively, 26 and 20 mm. Silicon-based filler is applied at the junction between P50 and SV2A material (~3 mm long). The position of the junction is the same as for the CMC–P50 sample. An additional block of P50 material is installed downstream from the third test sample. This second junction (SV2A–P50) is without filler.

In Fig. 4 (bottom), note that two Teflon plates with a thickness of ~1.45 mm are installed along the streamwise direction at sidewalls of the test sample. These technical solutions ensure a mechanical fixation of the sample on the FP holder.

3 Results

3.1 P50 test

Figure 5 shows two pictures extracted from the video sequence. The picture on the left corresponds to the beginning of the test when the sample is injected into the plasma flow. The picture on the right corresponds to the end of the test, i.e. 700 s after the sample injection. The plasma jet is coming from the right. The ablation products, which are released from the material, interact with the boundary layer and radiate. It is worth to note the wavelengths from these radiating species in the visible change after a certain exposure time when the char surface appears. After the plasma exposure, on the entire surface of the test sample a black char layer is formed and surface recession appears, more pronounced in the front part of the sample due to a higher heat flux (Fig. 6). The finely cracked top surface is characteristic of cork-based materials [9].

The mass loss of the sample has been obtained by weighing it before and after the test with a Kern EW150-3 M balance (reproducibility 2 mg, linearity ±3 mg). The mass loss of the P50 sample after 700 s of plasma exposure is 16.348 g which represent 26.5 % of the initial mass of the sample.

The temperatures acquired by the TCs with respect to the time are plotted in Fig. 7. The temperatures increase continuously during the plasma exposure. A temperature jump occurs in the first few seconds of the exposure. After this jump, the temperatures continue to increase at a lower rate. Starting from ~125 s, the temperature gradients of the TCs 1E, 2E and 5E are similar. However, the temperature gradient of the TC 3E is lower within the first ~130 s, and then it increases during the rest of the test duration. For the temperatures measured by the TCs, 1E and 2E, a plateau at the end of the test is reached. The maximum temperatures

Fig. 5 Images extracted from the video sequence of the P50 test at (*left*) start and (*right*) end

Fig. 6 Post-test pictures of the P50 sample

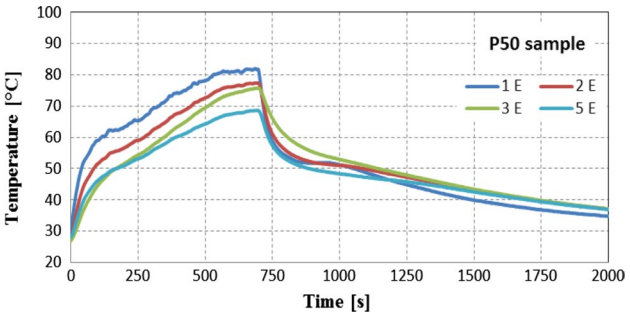

Fig. 7 Time evolution of the temperature acquired by the thermocouples for P50 sample

detected by the TCs, 1E, 2E, 3E and 5E, are 82, 77, 76 and 69 °C, respectively. The streamwise pattern of the temperatures measured by the TCs is in agreement with the heat flux distribution plotted in Fig. 1.

An overshoot is observed in the histories of the TCs, 1E and 2E, during the cooling down phase (~250 s after the end of the exposure to the plasma jet).

Figure 8 plots the temperature measured by the two-colour pyrometer with respect to the time. The blue markers correspond to the measurement points while the black curve represents a 5-order polynomial fit. The surface temperature at the measurement spot increases in the first 500 s of the test from ~850 °C up to ~992 °C. It slightly decreases in the last 200 s of the test. It is worthy to note that the large scattering of the measurement points of ±60 °C around the fit curve is observed.

Figure 9 shows the iso-contour of the IR temperature surface distribution at 350 s after the sample injection. The plasma flows from right to left. In the bottom, the

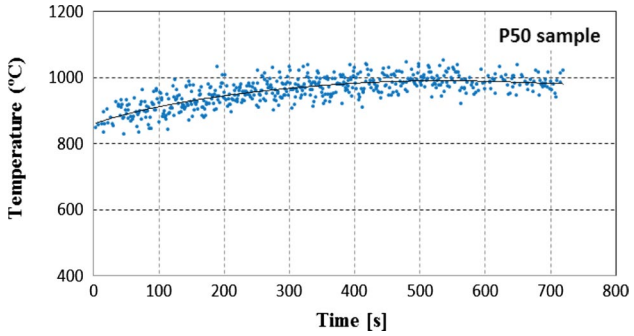

Fig. 8 Time evolution of the temperature acquired by the two-colour pyrometer for the P50 sample, with 5-order polynomial fit curve superimposed

temperature profile along the centreline of the sample is extracted from the IR temperature surface distribution. The axial-coordinate is the streamwise distance from the leading edge of the FP holder (Fig. 2).

The highest temperature of ~1100 °C is measured at ~71 mm from the FP leading edge. The surface temperature decreases to ~200 °C along the streamwise direction. Note that the temperatures measured by the two-colour pyrometer and IR camera ($\varepsilon_{IR} = 0.8$) at 350 s after the sample injection are in good agreement with each other. It implies that the emissivity of the P50 material at ~1000 °C is equal to the value of 0.8 in the spectral range and along the direction of the IR camera.

3.2 CMC–P50 test

In Fig. 10, the images extracted from the video sequence at beginning (left) and 700 s (right) from the injection of the test sample show that no visible radiating species are released from the CMC surface, since it is not an ablative material. Figure 11 shows post-test pictures of the CMC–P50 sample. As expected, the surface of the cork exposed to the plasma flow presents characteristic cracked char surface. As for the P50 sample, the recession of char surface in the upstream part with respect to the CMC plate is higher. Just downstream the CMC plate, the recession forms a rear-facing step (Fig. 11). A detailed post-test inspection of the junction between the CMC and the P50 material reveals that the slot geometry is well preserved. The P50 cork surface underneath the CMC plate is well preserved as well. The CMC plate shows different colour patterns at the surface. A bluish colour is also present on the two sides of the plate. It can be due to oxidation phenomena occurring over the surface of the CMC plate.

Since the test sample is composed of two separable parts, the mass loss is evaluated for each individual element. The mass loss for the P50 block is 13,834 g which represents 23.2 % of its initial mass. The mass loss of the

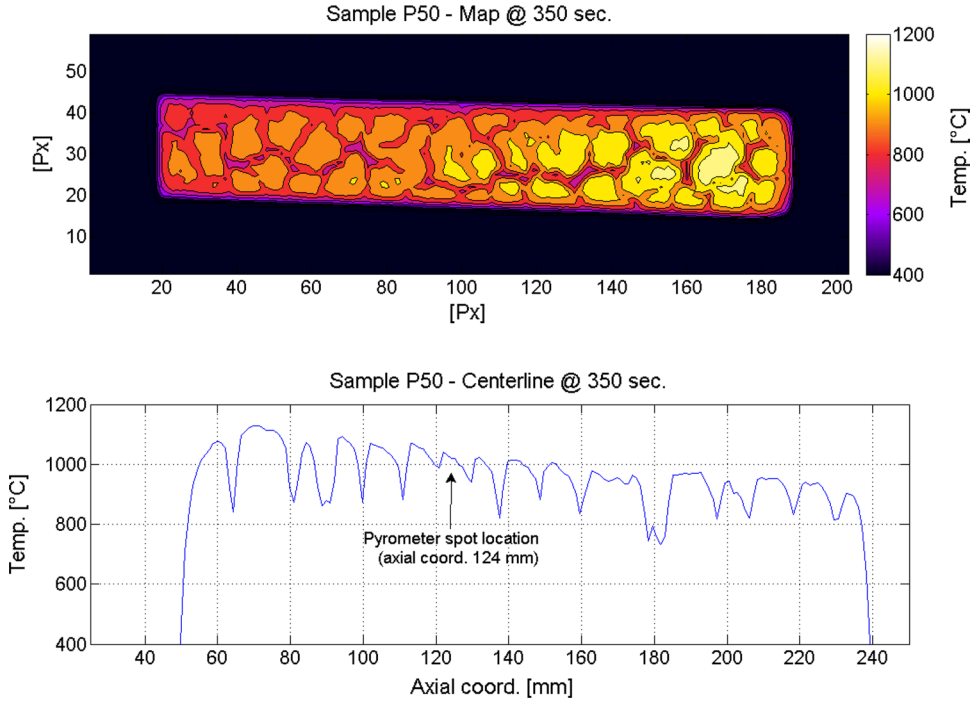

Fig. 9 Temperature surface distribution measured by IR camera ($\varepsilon_{IR} = 0.8$) at 350 s after sample injection for P50 sample: iso-contour (*top*), centreline distribution (*bottom*)

Fig. 10 Images extracted from the video sequence of the CMC–P50 test at (*left*) start and (*right*) end

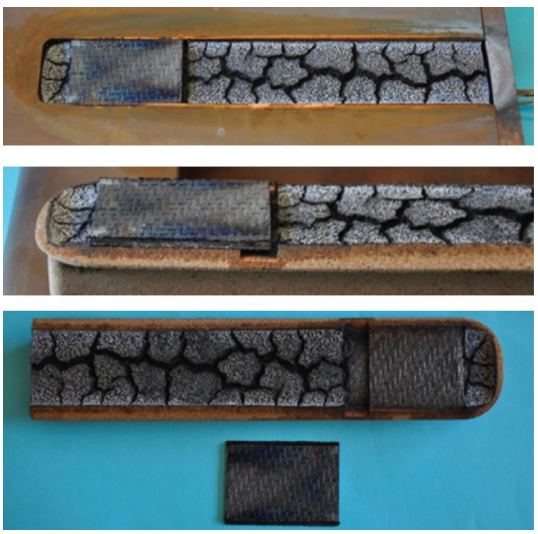

Fig. 11 Post-test pictures of the CMC–P50 sample

P50 material is lower than that measured in the P50 only test. The partial protection due to the CMC plate promotes the reduction of the mass loss. However, the CMC plate does not lose mass during the test.

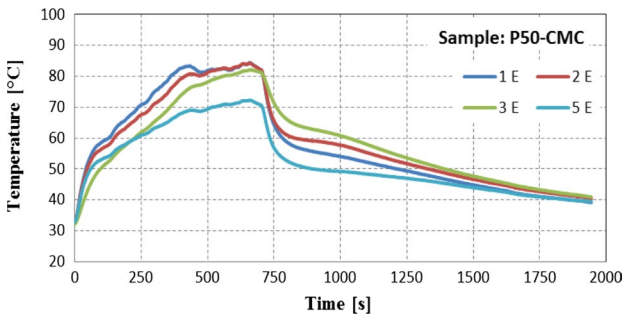

Fig. 12 Time evolution of the temperature acquired by the thermocouples for CMC–P50 sample

Figure 12 plots the time evolution of the temperatures acquired by the TCs for the CMC–P50 sample. As for the P50 test, the temperatures associated with the TCs 1E, 2E, 3E and 5E, show a similar trend. A temperature jump is measured in the first few seconds of the exposure. After this jump, the temperature continues to increase at a lower rate. Then the temperatures measured by the TCs 1E, 2E and 3E reach a plateau at the end of the test (~80 °C). Note that the maximum temperature at the back wall of the sample is less than the maximum allowable temperature of 150 °C at the cold structure. The temperature on the back wall of the test sample drops after the exposure time to the plasma jet. As for the P50 test, a slight overshoot is observed in the temperature time evolution after the plasma exposure. It is worth mentioning the initial temperature before the plasma exposure is higher of 5 °C in this test than for the P50 test, i.e. ~33 °C instead of 28 °C, respectively.

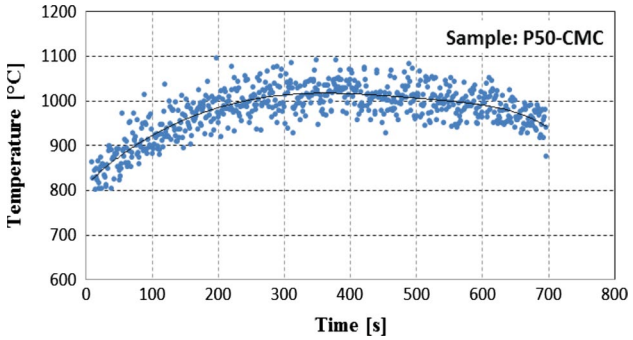

Fig. 13 Time evolution of the temperature acquired by the two-colour pyrometer for the CMC–P50 sample, 5-order polynomial fit curve is superimposed

In Fig. 13, the temperature measured by the two-colour pyrometer is plotted with respect to the time. The pyrometer points to the P50 material at 13 mm downstream the CMC–P50 interface (Fig. 2). The surface temperature downstream the junction increases up to a maximum value of ~1018 °C within the first 350 s. As for the P50 test, the pyrometer data show large amplitude fluctuations due to the disturbance of the IR signal due to the species released from the P50 material.

In Fig. 14, the iso-contour of the temperature distribution measured by the IR camera at 350 s after the injection of the CMC–P50 sample in the plasma jet is depicted. As for the P50 test, the temperatures measured by the two-colour pyrometer and IR camera ($\varepsilon_{IR} = 0.8$) are in good agreement to each other. It implies that the emissivity of the P50 material at ~1018 °C is equal to the value of 0.8 in the spectral range and along the direction of the IR camera. The maximum value of temperature reached at the surface of the CMC plate is of ~700 °C. In crosswise direction, the temperature distribution at the side wall of the CMC plate approaches to the surface temperature of the FP holder. It highlights the presence of heat sink caused by the contact of the dovetail joint of the CMC plate with the copper FP holder.

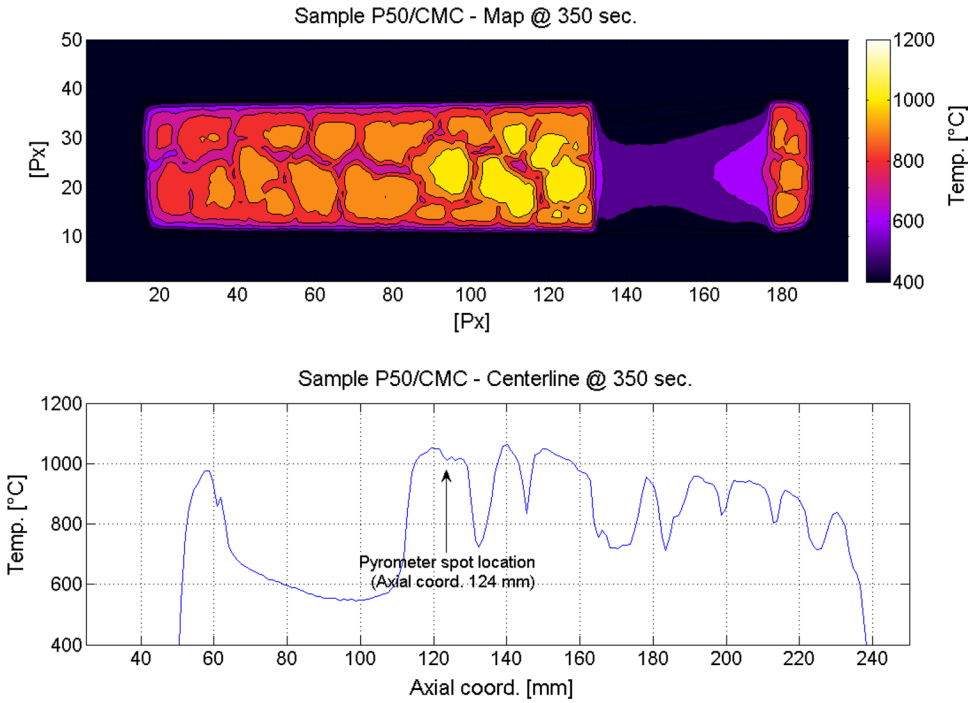

Fig. 14 Temperature surface distribution measured by IR camera ($\varepsilon_{IR} = 0.8$) at 350 s after sample injection for CMC–P50 test sample: iso-contour (*top*), centreline distribution (*bottom*)

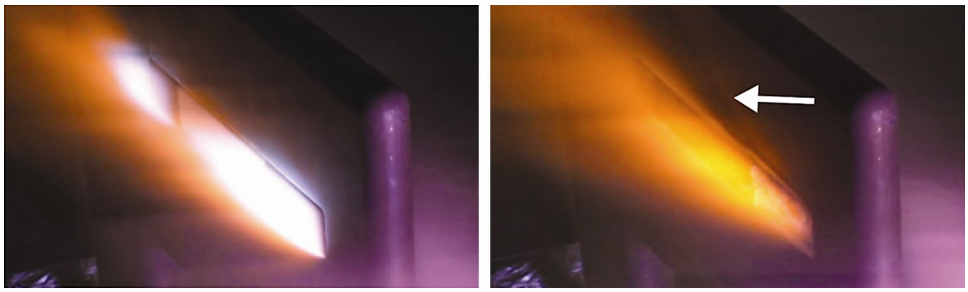

Fig. 15 Images extracted from the video sequence of the P50–SV2A test at (*left*) start and (*right*) end; the *white arrow* indicates the footprint of the wake flow on the surface of the FP holder during the plasma exposure

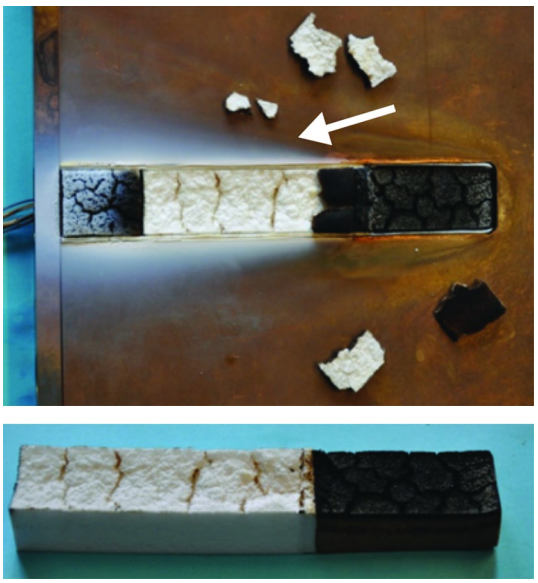

Fig. 16 Post-test pictures of the P50–SV2A sample; (*top*) the *white arrow* indicates the footprint of the wake flow on the surface of the FP holder

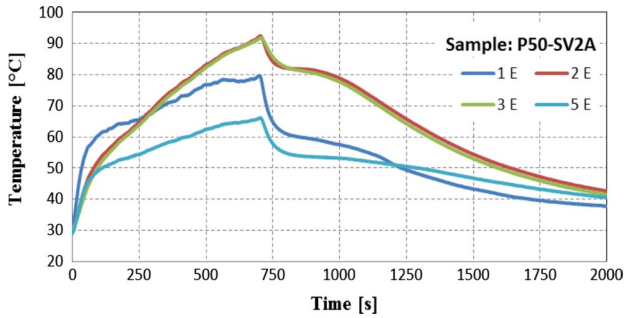

Fig. 17 Time evolution of the temperature acquired by the thermocouples for P50–SV2A sample

3.3 P50–SV2A test

In Fig. 15, the two pictures extracted from the video sequence reveal radiating species that emit in the visible as for the P50 test. Figure 16 shows post-test pictures of the P50–SV2A sample before and after disassembling. In the picture on top, several pieces of the SV2A char layer are detached from the sample. These pieces detach during the cooling down phase. The remaining SV2A charred layer just downstream the junction is also very loose. The surface of the P50 material exposed to the plasma flow presents characteristic cracked char surface. A large recession is observed in the upstream P50 part of the sample. The filler between the P50 and SV2A ablative materials does not show any sign of mechanical degradation. The side and bottom views of the test sample show that the thermal waves slightly penetrate in the ablative material and in the filler bond in between.

The mass loss for the block P50–SV2A is of 8.101 g which represents 16.1 % of its initial mass. The mass loss of the extra block in P50 material is 1.649 g which represents 17.6 % of its initial mass. It is worth to note Fig. 17 plots the time evolution of the temperature acquired by the TCs for the P50–SV2A test. The time evolution of the temperature acquired by the TCs 1E, 2E, 3E and 5E shows similar trends. The temperature gradients of the TCs 1E and 5E are similar during the plasma exposure. However, different levels are reached according to the actual heat flux applied at their position. Note that the temperature acquired by the TC 1E seems to stabilize at the end of the test. The TC 5E located at 211 mm from the leading edge of the FP is in contact with the extra P50 block. This block is exposed to the lowest heat flux and the TC 5E measures the lowest temperature. The maximum temperature measured by the TC 5E is of ~67 °C. The highest maximum temperature is detected by the TCs 2E and 3E. The TC 2E is in direct contact with the filler whiles the TC 3E is in contact with the SV2A material. These two TCs measure exactly the same temperature during the plasma exposure and during the cooling down phase. The maximum temperature reached at these two locations after 700 s of plasma exposure is of 93 °C; it is below the maximum allowable temperature of 150 °C for the cold structure.

Figure 18 plots the temperature measured by the two-colour pyrometer. The blue markers correspond to the

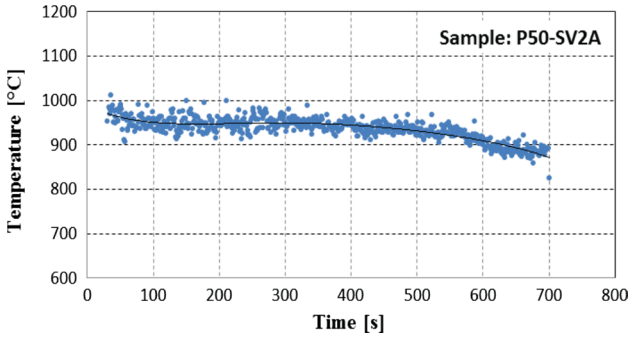

Fig. 18 Time evolution of the temperature acquired by the two-colour pyrometer for the P50–SV2A sample, 5-order polynomial fit curve is superimposed

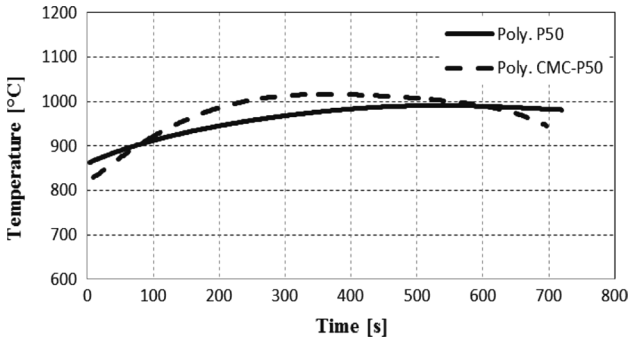

Fig. 20 Comparison plot of the 5-order polynomial curves by fitting two-colour data: *continuous line* P50 and *dotted line* CMC–P50

measurement points while the black curve represents to 5-order polynomial fit curve. The surface temperature at the target spot is almost constant (~950 °C) in the first 350 s of the test, before decreasing in the second half (~875 °C). The fluctuations of the pyrometer signal are lower for this test than for the P50 and CMC–P50. In this test, the measuring spot is on the surface of the SV2A block, instead of the P50. The ablation products released from the SV2A material disturb less the pyrometer signal in its infrared bandwidth (~1 μm).

In Fig. 19, the iso-contour of the temperature distribution measured by the IR camera at 350 s after the injection of the sample in the plasma jet is depicted. The transition P50 to SV2A results in a temperature drop at 110 mm from the leading edge of the FP holder. Note that the temperatures measured by the two-colour pyrometer and IR camera ($\varepsilon_{IR} = 0.8$) are in good agreement to each other. It implies that the emissivity of the SV2A material at ~950 °C is equal to the value of 0.8 in the spectral range and along the direction of the IR camera.

3.4 TPS interface effects

Figure 20 shows a comparison plot obtained by superimposing 5-order polynomial fit curves for the P50 and CMC–P50 tests.

As previously shown for the P50 test, the temperature measured by the two-colour pyrometer reaches a maximum value about of 992 °C. Assuming the radiative equilibrium condition is locally achieved, the heat flux re-irradiated

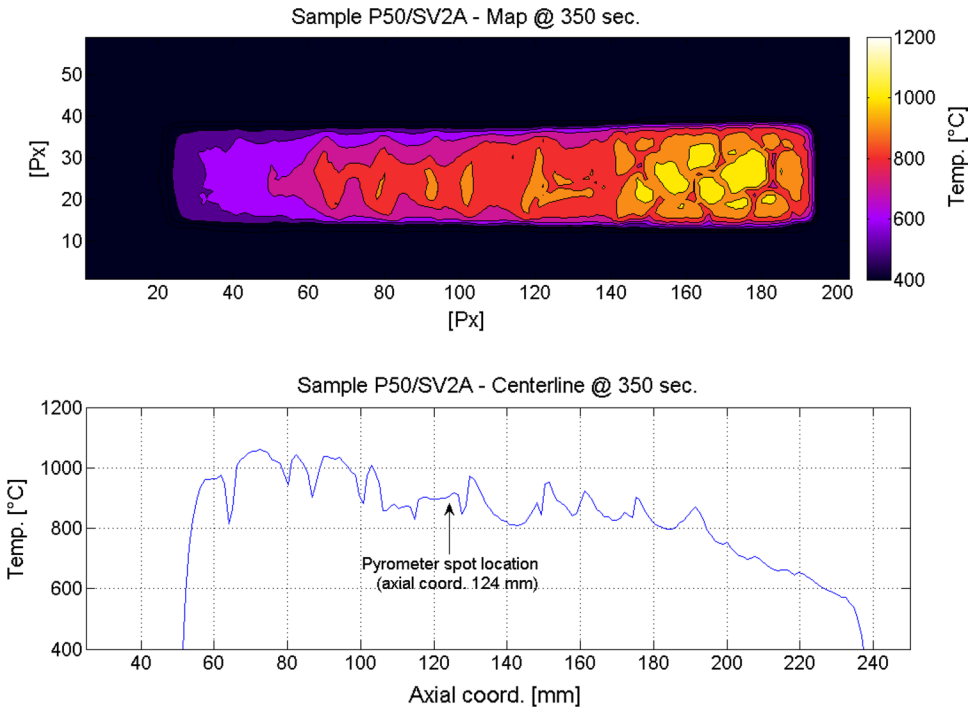

Fig. 19 Temperature surface distribution measured by IR camera ($\varepsilon_{IR} = 0.8$) at 350 s after sample injection for P50–SV2A test sample: iso-contour (*top*), centreline distribution (*bottom*)

from the surface Q_{rad} is about of 116 kW/m^2, estimated by the Stefan–Boltzmann law (Eq. 1).

$$Q_{rad} = \sigma \varepsilon T_w^4 \quad (1)$$

where σ is the Stefan–Boltzmann constant, T_w is the wall temperature and ε is the total hemispherical emissivity. For all the investigated materials, it is assumed that ε is equal to 0.8, i.e. the value found out in the spectral range and direction of the IR camera.

For the P50 test (11.7 MJ/kg, 1500 Pa), the calibrated heat flux [7] impinging at the location of the two colour pyrometer spot is of 160 kW/m^2 at cold wall condition (70 °C). However, the impinging heat flux decreases to 147 kW/m^2 at hot wall condition (T_w = 992 °C) according to the Fay-Riddell formula (Eq. 2) [10].

$$Q_w \propto H_0 - c_p T_w \quad (2)$$

where H_0 is the total enthalpy at boundary layer, c_p is the specific heat at constant pressure of the plasma (1.01 kJ/kgK). Comparing the impinging heat flux at hot wall condition with respect to the heat flux re-irradiated from the surface, it is possible to find out that the contribution of ablation and conduction to the heat flux balance is about 31 kW/m^2. Thus, the re-irradiated heat flux is 79 % of the impinging one and the rest can be considered as ablation and conduction.

Furthermore, the catalytic jump due to the CMC–P50 interface can be evaluated by comparing re-irradiated heat fluxes related to the maximum temperatures detected by the two-colour pyrometer for the CMC–P50 and P50 tests. As previously mentioned, the maximum temperature reached at the pyrometer spot location for the CMC–P50 test is 1018 °C. Assuming that the radiative equilibrium condition is locally achieved also for CMC–P50 test, the re-irradiated heat flux is 126 kW/m^2. Thus, the effect on the re-irradiated heat flux due to the catalytic jump at the CMC–P50 interface is about +10 %; it is reasonable to assume that the impinging heat flux accordingly increases. This overheating promotes also an increase of the recession rate according to the rear-facing step previously observed downstream from the interface for the CMC–P50 test (Fig. 11). In Fig. 20, this overheating is inhibited after 600 s; the final temperature for the CMC–P50 sample is lower than for the P50 sample. It can be due to a wake flow occurring in correspondence of the rear-facing step.

In Fig. 18, the temperature reached on SV2A material during the plateau phase is about 950 °C. In radiative equilibrium condition at the pyrometer spot location, the heat flux re-irradiated from the surface is 102 kW/m^2. The impinging heat flux decreases about to 148 kW/m^2 at hot wall condition (950 °C) (Eq. 2). For the SV2A material, the contribution of ablation and conduction to the heat flux balance is about 46 kW/m^2: roughly 69 % of the impinging heat flux is balanced by re-irradiation and 31 % by ablation and conduction. Furthermore, the maximum temperature detected at the first 30 s from the injection of the SV2A sample into the plasma flow is associated with the swelling of the SV2A material. It promotes the formation of a wake flow induced by the new shape of the P50–SV2A sample. The wake flow is also visible in Fig. 15 (right). In Fig. 16, the deposition of white particles coming from the upstream silicon-based filler on the surface of FP holder gives a qualitative visualization of the spreading of the wake. In addition, these residual particles coat the surface of the SV2A block and of the P50 one downstream.

4 Conclusions

Three test samples have been tested in off-stagnation configuration in Plasmatron facility at VKI in the framework of the IXV TPS activities. Two interfaces representative of the real TPS assemblies of the IXV have been investigated. The first junction is composed of an upstream CMC plate and an ablative P50 cork composite block separated with a gap of 2 mm. The second one is made of an upstream P50 block and an ablative SV2A silicon elastomer-based material block with silicon filler in between. A sample composed of P50 material is tested in order to obtain reference results without TPS interface effects.

The three test samples have withstood relatively well the imposed heat flux. The qualification tests highlight the thermal behaviour of the TPS interfaces under flight representative conditions in terms of heat flux and integral heat load (~180 kW/m^2 for 700 s). Both ablative tested materials, P50 and SV2A, undergo an expected thermal degradation with the formation of a porous char layer. Recession of the char layer is detected for the P50 material. On the other hand, SV2A material swells in the first few seconds during the plasma exposure. The silicon-based filler applied between the P50 and SV2A materials exhibits effects of thermal degradation on the surface. Heat sink effect due to the dovetail joint between the CMC plate and FP holder is observed. The maximum temperatures measured by the TCs at the rear wall of the CMC–P50 and P50–SV2A interfaces, respectively, of 80 and 93 °C, are less than the maximum allowable temperature of 150 °C at the cold structure.

For the P50 material, the re-irradiated heat flux contributes 79 % of the impinging heat flux. For the SV2A material, the re-irradiated heat flux contributes 69 % of the impinging heat flux. Recession/swelling behaviour has been observed as characteristic of the P50–SV2A junction when exposed to the plasma flow. For the CMC–P50 test, the catalytic jump due to the CMC–P50 interface determines an overheating about of +10 % in terms of

re-irradiated heat flux. A pronounced recession of the P50 material nearby the junction has been observed.

The results definitely highlight the fact that the ground testing data are necessary for the development and qualification of TPS and their interfaces for re-entry applications. Indeed the path towards the complete understanding of the variation of the heat flux at the interface between TPS materials with different catalytic properties is still steep. A further investigation is envisaged through the cross-analysis of the flight data gathered during IXV mission and of the ground testing data. The use of these new insight promises to reduce the margins on TPS design for future re-entry missions.

References

1. Rakich, J.V., Stewart, D.A., Lanfranco, M.J.: Results of a flight experiment on the catalytic efficiency of the space shuttle heat shield. AIAA Pap. **81**, 0944 (1982)
2. Anderson, J.D.: Hypersonic and High Temperature Gas Dynamics. McGraw Hill, New York (1989)
3. Panerai, F.: Aerothermochemistry characterization of thermal protection systems. Dissertation, Ph.D. thesis, Università degli Studi di Perugia, von Kármán Institute for Fluid Dynamics (2012)
4. Panerai, F., Chazot, O.: Plasma wind tunnel testing as support to the design of gas-surface interaction in-flight experiments. In: Proceedings of 17th AIAA International Space Planes and Hypersonic Systems and Technologies Conference, AIAA 2011–2276, San Francisco, CA, USA (2011)
5. Bottin, B., Carbonaro, M., Zemsch, S., Degrez, G.: Aerothermodynamic design of an inductively-coupled plasma wind tunnel. In: Proceedings of 32nd Thermophysics Conference, AIAA 97–2498, Atlanta, USA (1997)
6. Chazot, O., Panerai, F., Van Der Haegen, V.: Off-stagnation point testing and methodology in plasma wind tunnel. In: Proceedings of 17th AIAA International Space Planes and Hypersonic Systems and Technologies Conference, AIAA 2011–2210, San Francisco, CA, USA (2011)
7. Viladegut, A.: Off-Stagnation Point Testing in Plasma Wind Tunnel for Ground-to-Flight Extrapolation, VKI Project Report, Von Kármán Institute for Fluid Dynamics (2012)
8. Pinaud, G., van Eekelen, A.J.: Aerofast: development of cork TPS material and a 3D comparative thermal/ablation analysis of an Apollo and a biconic sled shape for an aerocapture mission. In: Proceedings of 8th IPPW-8 International Planetary Probe Workshop, Portsmouth, VA, USA (2011)
9. Hovey, R.W.: Cork thermal protection design data for aerospace vehicle ascent flight. J. Spacecr. Rockets **2**(3), 300–304 (1965)
10. Fay, J., Riddell, F.R.: Theory of stagnation point heat transfer in dissociated air. J. Aero. Sci. **25**(2), 73–85 (1958)